



<http://www.diva-portal.org>

Postprint

This is the accepted version of a paper published in *IEEE transactions on energy conversion*. This paper has been peer-reviewed but does not include the final publisher proof-corrections or journal pagination.

Citation for the original published paper (version of record):

Falk Olson, G., Wu, Y., Peretti, L. (2023)

Parameter Estimation of Multiphase Machines Applicable to Variable Phase-Pole Machines

*IEEE transactions on energy conversion*, : 1-10

<https://doi.org/10.1109/tec.2023.3288368>

Access to the published version may require subscription.

N.B. When citing this work, cite the original published paper.

Permanent link to this version:

<http://urn.kb.se/resolve?urn=urn:nbn:se:kth:diva-329847>

# Parameter Estimation of Multiphase Machines Applicable to Variable Phase-Pole Machines

Gustaf Falk Olson, *Student Member, IEEE* and Yixuan Wu, *Student Member, IEEE* and Luca Peretti, *Member, IEEE*

**Abstract**—Variable phase-pole machines are envisioned in applications requiring a large torque-speed operating area. The control of these machines relies on accurate models and parameters but research on their parameter identification is scarce. This paper presents an offline parameter-identification method for variable phase-pole machines adopting a harmonic-plane decomposition model. The method employs standard tests with single-frequency three-phase excitation in multiple pole configurations and uses the results to minimize a constrained, regularized weighted least-squares problem. It relies on identifying a set of parameters common to all phase-pole configurations and transforming them into the adopted model. Good agreement is exhibited when comparing experimental results to an analytical harmonic-plane decomposition model using the inferred parameters. Steady-state, as well as pole transitions, are compared. The paper emphasizes the importance of performing measurements in multiple pole configurations and weighing these measurements appropriately to render an accurate set of parameters.

**Index Terms**—parameter estimation, harmonic plane decomposition, multiphase electric machines, variable phase-pole machine

## I. INTRODUCTION

THE vector-space decomposition (VSD) is the state-of-the-art method for modeling space vectors in multiphase electrical machines (MPEMs) [1]. In the VSD, time-domain space-vectors quantities map into orthogonal vector spaces. A drawback is that the number of vector spaces,  $\lceil m_s/2 \rceil$ , increases with the number of phases,  $m_s$ . As a result, the number of controllers in a MPEMs with phase-changing capabilities ought to change with the number of phases [2]. The number of spaces depends on  $m_s$  because the VSD assumes  $m_s$  fixed magnetic axes. This is a viable approach when the currents in a phase belt are equal, i.e the conductors in the slots belonging to the same phase belt are series-connected.

So-called variable phase-pole machines (VPPMs) of induction type are capable of varying the number of poles and phases by controlling the current in independent stator slot groups [3]–[6]. The phase-pole configuration (PPC) is chosen to fulfill some optimality criterion, e.g maximum-torque-per-ampère, making the operation of a VPPM similar to an electric gear box. As compared to fixed phase-pole induction machines (IMs), the literature reports that VPPMs improve light-load efficiency of the inverter/machine [7], reduce the DC-link capacitance [7], and enlarges the torque-speed operating area for a given machine and inverter size [6]–[8]. A case study in [8] shows that a VPPM achieves better machine efficiency in the high-speed region than an interior permanent

magnet motor. Additionally, the mentioned VPPMs are free of magnets. All of the above capabilities position VPPMs as a contender for traction applications. By construction, however, they do not necessarily generate equal and opposite currents in the slots shifted by  $\pi$  rad electrically. Moreover, the number of magnetic axes depends on the winding arrangement, the number of independent coils, and their excitation [2].

A generalized VSD, the harmonic plane decomposition (HPD), was introduced in [2] to establish a model with a fixed number of subspaces for VPPMs. This model is consistent independently of the configuration. The HPD accomplishes this by considering all possible magnetic axes in isolation. The number of subspaces is  $\lceil n_{mw}/2 \rceil$  for a machine with  $n_{mw}$  independently excitable windings, referred to as *minimum windings*. Thus, the number of subspaces only depends on  $n_{mw}$ . In case of a  $Q_s$  stator-slot VPPM with independent coil excitation, there are  $\lceil Q_s/2 \rceil$  independent subspaces. Therefore, it removes the need to adjust the model, controllers, transformation matrices, and their parameters, which has previously been necessary [7], [9]. Irrespective of the model, however, the performance of the drive and the model fidelity depends on the parameter accuracies.

Parameter identification (ID) for three-phase IMs find practical use in establishing accurate field orientation under varying load conditions and magnetization, controller tuning, compliance testing, and fault analysis. The literature on multiphase IMs is less extensive but encompasses some analytical [10] and finite element methods (FEMs) [11], as well as online and offline tests [12], [13]. Many studies on parameter-ID methods of MPEMs assume that the stator winding is sinusoidally distributed. This means that the VSD model neglects the magnetic coupling between the stator and rotor except in the first (fundamental) vector space. This simplification reduces the effort to estimate the VSD parameters so that standard no-load (NL) and locked-rotor (LR) tests with mixed-frequency excitation suffice to deduce the parameters [13]. However, it may be inaccurate and inappropriate if, for example, harmonics are injected to assist in the torque production, or when considering VPPMs [14].

In contrast, [15] introduces a model where low-order space-harmonics in a six-phase IM are incorporated into an adapted VSD model. A method to compute parameters in subspaces other than the fundamental is proposed. A similar method is employed for an eleven-phase IM in [16], but the magnetizing inductances are here estimated experimentally for all subspaces of interest. Through complementing physical considerations, the paper highlights the important interdependence between sequence parameters, which is used to estimate the

G. Falk Olson, Y. Wu and L. Peretti are with the department of electrical energy conversion at the Royal Institute of Technology, KTH, in Stockholm, Sweden (e-mails: {gufo, yixuanw, luca}@kth.se).

rotor parameters of higher-order subspaces from one LR test. [10] establishes analytical equations for the VSD-parameters of a VPPM where the number of phases varies and the winding pole count is unequal to the magnetic pole count. It verifies them by means of standard NL and LR tests performed on a FEM-model. [11] elaborates a FEM to deduce the pole-/harmonic order-dependent parameters of a multiphase IM, which is an important basis for FEM-estimation of the parameters of a coherent VPPM model, such as the HPD. A FEM directly targeted to identify the HPD parameters of a toroidally-wound VPPM is declared in [17]. Still, a robust and light (in terms of number of experiments) method to experimentally identify the parameters of an invariant VPPM model appears to be missing in the literature.

To this end, this paper proposes a method to identify the full suite of HPD parameters of all PPCs of a VPPM from a limited number of NL and LR tests under fundamental excitation. It is an extension of the previously published conference paper [18] and elaborates on the parameter-estimation theory. It adds experimental support to assess the accuracy of the identified parameters in the HPD model. The effect of rotor skewing is incorporated and practical guidance is given to accomplish fair validations of the parametric model.

The VPPM under study is presented in [4], [17]. It is similar in construction to [6], [19]. Section II presents the machine model. Section III introduces the set of parameters to be estimated and the relationship between them and the parameters of the T-equivalent VSD and HPD models. Moreover, the parameter ID-method is introduced. Section IV reports the identified parameters of the considered VPPM. Section V compares experimental data to an analytical HPD model using the inferred parameters from Section IV. NL curves, loaded steady-state (s.s) response, and phase-pole transitions are used in the assessment. Section VI summarizes the main findings.

## II. MACHINE MODEL

The amplitude-invariant HPD transformations, (1), transform space-vector quantities between the fundamental reference frame [20],  $\mathbf{x}_{123}$ , and  $\xi = \lceil n_{mw}/2 \rceil$  independent stator-referenced subspaces.  $T$  denotes transpose.  $K_{mw} = 1$  indicates machine coils and  $K_{mw} = 0.5$  toroidal windings.

$$\mathbf{x}_{\alpha\beta} = \underbrace{2/n_{mw}}_{\mathbf{T}_{123 \rightarrow \alpha\beta}} \mathbf{C} \cdot \mathbf{x}_{123}, \quad \mathbf{x}_{123} = \underbrace{\mathbf{C}^T}_{\mathbf{T}_{\alpha\beta \rightarrow 123}} \cdot \mathbf{x}_{\alpha\beta}$$

$$\mathbf{C} = \begin{bmatrix} 1 & \cos(\delta) & \cos(2\delta) & \dots & \cos(\delta(n_{mw} - 1)) \\ 0 & \sin(\delta) & \sin(2\delta) & \dots & \sin(\delta(n_{mw} - 1)) \\ 1 & \cos(2\delta) & \cos(4\delta) & \dots & \cos(2\delta(n_{mw} - 1)) \\ 0 & \sin(2\delta) & \sin(4\delta) & \dots & \sin(2\delta(n_{mw} - 1)) \\ \vdots & \vdots & \vdots & \ddots & \vdots \\ 1 & \cos(\xi\delta) & \cos(2\xi\delta) & \dots & \cos(\xi\delta(n_{mw} - 1)) \\ 0 & \sin(\xi\delta) & \sin(2\xi\delta) & \dots & \sin(\xi\delta(n_{mw} - 1)) \end{bmatrix} \quad (1)$$

$$\delta = \pi/(K_{mw}n_{mw})$$

Using the discrete Fourier-transformation interpretation of the HPD, [2], it is realized that the transformation decomposes the space-vector quantity into space-harmonic components. A consequence is that the same time-harmonic component may map into several harmonic planes [2][(3)]. Hence, the

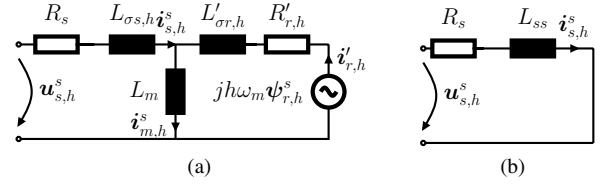


Fig. 1: HPD T-equivalent circuits (a) with rotor and (b) without rotor in a stator-oriented reference frame.

HPD decodes information about the amplitude and phase of these space harmonics that arise due to the different time harmonic components. As shown in [2], the number of HPD subspaces is solely dependent on the number of independent windings, contrary to the VSD. However, the lumped-parameter equivalent model-structures are analogous [2]. Moreover, the parameters don't change with the PPC. Rather, different harmonic planes are excited to emulate the desired PPC by means of current control. This is considered a virtue, as it avoids model discontinuities which arise if a phase-dependent VSD model is adopted [2], [7].

Employing the T-equivalent model in Fig. 1, each harmonic plane comprises a stator resistance,  $R_{s,h}$ , and a stator leakage inductance,  $L_{\sigma s,h}$ . A magnetizing inductance  $L_{m,h}$ , a rotor leakage inductance,  $L'_{\sigma r,h}$ , and a rotor resistance,  $R'_{r,h}$ , also exist in the planes where the stator couples to the rotor. When the number of rotor bars  $Q_r < Q_s$ , this is true for harmonic planes  $h \leq \lfloor Q_r/2 \rfloor$ , due to the Nyquist-Shannon theorem [2].

In Section V, simulations of an HPD model are compared to experiments. We then use the electrical stator-referred machine equations, (2), of the T-equivalent circuit in Fig. 1. Here,  $\omega_m$  is the rotor mechanical frequency.  $\psi_{(\cdot),h}^s$ ,  $\mathbf{u}_{(\cdot),h}^s$ ,  $\mathbf{i}_{(\cdot),h}^s$  denote complex space vectors of the flux linkage, voltage, and current in the stator reference-frame of harmonic plane  $h$ .  $s$ ,  $r$ , or  $m$  replace  $(\cdot)$  for stator, rotor and magnetizing quantities.  $K_{mw} = 1$  and  $K_{mw} = 0.5$  for conventional and toroidal windings, respectively [2].  $(*)$  denotes the complex conjugate.

$$\begin{aligned} d\psi_{s,h}^s/dt &= \mathbf{u}_{s,h}^s - R_{s,h}\mathbf{i}_{s,h}^s \\ d\psi_{r,h}^s/dt &= jh\omega_m\psi_{r,h}^s - R'_{r,h}\mathbf{i}_{r,h}^s \\ \tau_e &= \frac{K_{mw}n_{mw}}{2p_{mw}} \sum_{h=1}^{\lfloor n_{mw}/2 \rfloor} \frac{hL_{m,h}}{L_{m,h} + L'_{\sigma r,h}} \text{Im} \{ \psi_{r,h}^{s*} \mathbf{i}_{s,h}^s \} \quad (2) \\ \mathbf{i}_{m,h}^s &= \mathbf{i}_{s,h}^s + \mathbf{i}'_{r,h} \\ \psi_{s,h}^s &= L_{m,h}\mathbf{i}_{m,h}^s + L_{\sigma s,h}\mathbf{i}_{s,h}^s, \quad \psi_{r,h}^s = L_{m,h}\mathbf{i}_{m,h}^s + L'_{\sigma r,h}\mathbf{i}'_{r,h} \end{aligned}$$

Furthermore, (3) declares the slip of  $h$  with  $\omega_{sl,h}$  denoting the slip frequency.  $\nu_h$  is the order and sequence of the VSD vector space that maps into  $h$ , as explained in [2].

$$s_h(\nu_h, \omega_s, \omega_m) = (\nu_h\omega_s - h\omega_m)/(\nu_h\omega_s) = \omega_{sl,h}/(\nu_h\omega_s). \quad (3)$$

## III. VSD- AND VPPM-MODEL PARAMETERS

This chapter establishes analytical formulae to express the HPD parameters as functions of the space-harmonic orders, i.e.  $h$ . Magnetic linearity is assumed, implying no mutual interaction between the harmonic planes. Relations between the three-phase VSD and HPD parameters are stated. The goal is to identify the VSD parameters using standard single-frequency excitation tests, whereby we elaborate an equivalent HPD model. A Bayesian weighted least-squares (WLS)

optimization is used to deduce all HPD parameters based on measurements and the presented analytical relations.

### A. Stator Parameters and Magnetizing Inductance

The stator resistance,  $R_{s,h}^{\text{HPD}}$ , is equal for all harmonic planes, which follows from the transformations in [17]. It is effectively the DC resistance of one independent winding, which can be measured with an Ohm-meter. Conversely,  $R_{s,h}^{\text{VSD}}$  is the sum of series-connected independent windings.

The stator inductance,  $L_{ss}^{\text{VSD}}$ , comprises terms corresponding to the flux linkage between the stator and rotor, as well as leakage flux paths. Eq. (4) expresses it as a sum of the magnetizing and air-gap leakage inductance,  $L_{sd,p}^{\text{VSD}} = L_{m,p}^{\text{VSD}} + L_{\delta,p}^{\text{VSD}}$ , and a lumped leakage inductance,  $L_{\sigma's}^{\text{VSD}}$ , comprising the slot,  $u$ , tooth-tip,  $t$ , and end-winding leakage,  $w$  [21].

$$L_{ss,p}^{\text{VSD}} = L_{sd,p}^{\text{VSD}} + L_{\sigma's}^{\text{VSD}} \quad (4a)$$

$$L_{sd,p}^{\text{VSD}} = Q_s/m_s \sum_{h \in h_{1,p}} (k_{d,h}/h)^2 L_{m,1}^{\text{HPD}} \quad (4b)$$

$$L_{\sigma's}^{\text{VSD}} = Q_s/m_s \cdot z_Q^2 \mu_0 [l'(\lambda_u + \lambda_t) + l_w \lambda_w] = Q_s z_Q^2 \Lambda_\sigma / m_s \quad (4c)$$

In the above expressions,  $\lambda_{(\cdot)}$  denote permeance factors,  $z_Q$  the number of series-connected conductors per slot,  $l'$  the active length, and  $l_w$  the end-winding length.  $k_{d,h}$  is the distribution factor of the  $h^{\text{th}}$  harmonic plane for the current distribution (or equivalently: PPC) of interest. The index  $p$  indicates the pole configuration of the VPPM when the coils are series-connected.  $h_{1,p} = p(6k \pm 1)$  for  $k \in \mathbb{N}$  is interpreted as the set of harmonic planes containing the fundamental time harmonic for the  $[m_s = 3, p = 1]$  PPC. For instance,  $h_{1,1} = \{1, 5, 7, \dots\}$  yields the familiar sequence of space harmonics for a  $[m_s = 3, p = 1]$  machine. In this case, the physical configuration determines the space-harmonic orders of the air-gap magnetic field. The sum is supposed to be taken over all possible harmonics. For simplicity, we decide to truncate the sum to the highest space-harmonic order resolvable by the HPD,  $h = \lceil n_{mw}/2 \rceil$ .

The summation in (4b) results in the equivalent  $L_{sd,p}^{\text{VSD}}$  of the VSD-model for the fundamental vector space. The first term corresponds to the magnetizing inductance which couples the stator and the rotor, whereas the higher order terms constitute air-gap leakages [21][ch. 4.3.2]. For the machine under study,  $Q_s/m_s$  is the turns number. Based on (4b), the magnetizing inductance of the  $h^{\text{th}}$  plane is defined in (5). From (4), they obey the relation in (6). It is pointed out that only the first  $Q_r/2$  planes present a coupling between the rotor and stator and only leakages are present in  $h > Q_r/2$ .

$$L_{m,h}^{\text{HPD}} := L_{m,1}^{\text{HPD}} / h^2 \quad (5)$$

$$L_{m,p}^{\text{VSD}} = Q_s k_{d,p}^2 / m_s L_{m,p}^{\text{HPD}} \quad (6)$$

Unlike a conventionally wound stator winding where the coils belonging to a phase form  $2p$  series-connected end-winding bundles of  $z_Q q_s$  turns, a toroidally wound stator has distinct coils of  $z_Q$  turns. The end-winding consists of a series-connection of  $Q_s/m_s$  of these coils. It justifies the modification of the inductance expression [21][(4.98)] in (4c) and allows to lump the permeances of the slots, tooth tips, and end-windings into one equivalent permeance,  $\Lambda_\sigma$ . The expression can still be

used for VPPMs with conventional windings, but the last term within the brackets should be multiplied with  $q_s$ . However, this has no effect on the last equality since a new permeance, still proportional to the scaling factor  $Q_s z_Q^2 / m_s$ , can be defined.

Eq. (4) indicates that the leakage can be split into terms that either depend on the space-harmonic order,  $L_{\delta,p}$ , or not,  $L_{\sigma's}$ . The permeance  $\Lambda_\sigma$  depends on the machine's geometry and magnetic properties and is independent of the winding configuration. So, if the permeance of a slot, tooth-tip, and end-winding portion can be estimated, the HPD-inductances can be calculated by adjusting the scaling factor  $Q_s z_Q^2 / m_s$ .

### B. Rotor Parameters

In [17], an analytical relation between the space harmonic order and the rotor resistance,  $R'_r$ , and rotor leakage inductance,  $L'_{\sigma r}$ , was used for a non-skewed squirrel-cage rotor. With  $\underline{Z}(\cdot) = R(\cdot)F_{sk,R} + j\omega_{sl}L(\cdot)F_{sk,L}$  denoting the complex bar ( $b \mapsto (\cdot)$ ) and end-ring ( $er \mapsto (\cdot)$ ) impedances, the relation can be written as a primary-referred rotor impedance, (7) [21].

$$\underline{Z}'_r = m_s (k_{d,p} N_s)^2 / [m_r (k_{sk,p} N_r)^2] \cdot \left[ \underline{Z}_b + \underline{Z}_{er} / (2 \sin^2 \frac{p\pi}{Q_r}) \right] \\ k_{sk,\nu} = \sin \nu \frac{\pi s_{sp}}{2 m_s q_s} / \left( \nu \frac{\pi s_{sp}}{2 m_s q_s} \right) \quad (7)$$

It is apt for the HPD-model since each HPD-plane encompasses a distinct space harmonic order. The skin-effect factors  $F_{sk,(\cdot)}$  are derived in [22][ch.2.6.2]. The skew-factor,  $k_{sk,\nu}$ , for the  $\nu^{\text{th}}$  pole-pair field of the incumbent configuration is developed in [21][Ch.4.3.1].  $s_{sp}$  signifies the skewing as the number of stator slot pitches,  $m_r = Q_r$  is the number of rotor phases, and  $N_s = z_Q Q_s (2m_s)^{-1}$  and  $N_r = 0.5$  are the number of turns of the stator and rotor, respectively.

From (7),  $L_b$ ,  $R_b$ ,  $L_{er}$ , and  $R_{er}$  can be considered a set of fixed rotor parameters that are independent of the winding configuration and frequency. However, the adopted winding configuration determines the transformer ratio whereas the dimension of the end-ring segment is a function of  $p$ . It causes the effective end-ring impedance, the second term in (7), to decrease for higher  $p$ .

### C. Relation Between VSD and HPD Parameters

Provided  $\mathbf{L}_m^{\text{HPD}} \in \mathbb{R}^{\lceil n_{mw}/2 \rceil}$ , and the scalars  $R_s^{\text{VSD}}$ ,  $\Lambda_\sigma$ ,  $L_b$ ,  $R_b$ ,  $L_{er}$  and  $R_{er}$ , the HPD-parameters of the T-equivalent model are computed by applying the appropriate turns ratios,  $k_{d,h}$  and  $k_{sk,h}$ -factors, and number of series-connected stator coils as follows.

The base configuration of the studied VPPM with  $n_{mw} = Q_s$  is equivalent to a  $m_b = Q_s$ -phase machine with  $N_s = z_Q/2$  turns per phase arranged as concentrated windings. Hence,  $k_{d,h} = 1, \forall h \in \{1, 2, \dots, Q_s/2\}$ . The division by two when calculating  $N_s$  is carried out because one phase of the wound independently-controlled stator-coils machine (WICSC machine) encompasses half a coil, c.f. the rotor where  $N_r = 0.5$ . By (7), the desired transformation into HPD rotor-parameters is given by (8). The skew factor for the HPD-model,  $k_{sk,h}^{\text{HPD}}$ , is obtained by substituting  $\nu \rightarrow h$ , and  $m_s q_s \rightarrow Q_s$ .

$$\underline{Z}'_{r,h}{}^{\text{HPD}} = Q_s z_Q^2 / [(k_{sk,h}^{\text{HPD}})^2 Q_r] \cdot \left[ \underline{Z}_b + \underline{Z}_{er} / (2 \sin^2 \frac{h\pi}{Q_r}) \right] \quad (8)$$

Next, the stator inductance is declared in (9).

$$L_{ss,h}^{HPD} = L_{m,h}^{HPD} + L_{\sigma s}^{HPD} = L_{m,h}^{HPD} + z_Q^2 \Lambda_\sigma \quad (9)$$

The relations above suggest how to transform the basic parameters into HPD T-model equivalents. However, it is necessary to confirm that the resulting HPD-parameters render a model that is equivalent to the VSD model. To do so, one can consider the energy-conservation equality in (10).

$$m_s L_{ss,p}^{VSD} |i_s^{VSD}|^2 / 2 = m_b \sum_{h \in h_p} L_{ss,h}^{HPD} |i_{s,h}^{HPD}|^2 / 2 \quad (10)$$

Utilizing the relations (4),  $m_b = Q_s$ , and  $i_{s,h}^{HPD} = k_{d,h} i_{s,h}^{VSD}$ , and rearranging (10) yields (11). Comparing to (4), the three terms are identified as  $L_{m,p}^{VSD}$ ,  $L_{\delta,p}^{VSD}$ , and  $L_{\sigma' s,p}^{VSD}$ .

$$\begin{aligned} L_{ss,p}^{VSD} &= Q_s / m_s \left( k_{d,p}^2 L_{m,p}^{HPD} + \sum_{\substack{h \in h_{1,p} \\ h \neq p}} k_{d,h}^2 L_{m,h}^{HPD} + z_Q^2 \Lambda_\sigma \right) \\ &= Q_s / m_s \sum_{h \in h_{1,p}} |k_{d,h}|^2 L_{ss,h}^{HPD} \end{aligned} \quad (11)$$

Similarly, by considering the conservation of stator Ohmic losses, the stator resistance of the HPD-model is related to the stator resistance of the VSD-model as in (12).

$$R_{s,h}^{HPD} = m_s / Q_s \cdot R_s^{VSD}, \quad \forall h \in \{1, 2, \dots, Q_s/2\} \quad (12)$$

### D. Parameter Estimation Method

Since the analysed VPPM can be configured as a  $[m_s = 3, p = \{1, 2, 3, 6\}]$  machine, it is possible to run standard tests in these configurations and formulate (overdetermined) linear equation systems (LESs) using (4), (6) and (7) where the unknown parameter vector is  $\theta^T = [(\mathbf{L}_m^{HPD})^T \ \Lambda_\sigma \ L_b \ L_{er} \ R_b \ R_{er}]$ . Hereinafter, estimators of the parameters in  $\theta$  are denoted with  $\hat{\cdot}$

DC values of  $R_b$  and  $R_{er}$  are derived from a least-squares (LSQ) minimization of the LES in (13).  $L_b$  and  $L_{er}$  are related to  $L'_{\sigma r}$  in the same way. The HPD parameters ensue from (8).

$$\underbrace{\begin{bmatrix} R_{r,1}^{VSD} \\ R_{r,2}^{VSD} \\ R_{r,3}^{VSD} \\ R_{r,6}^{VSD} \end{bmatrix}}_{\mathbf{b}_r} = \underbrace{\frac{4m_s N_s^2 F_{sk,R}}{Q_r} \begin{bmatrix} \frac{k_{d,1}^2}{k_{sk,1}^2} |p=1, \frac{k_{d,1}^2/k_{sk,1}^2 |p=1}{2 \sin^2 \pi/Q_r} \\ \frac{k_{d,1}^2}{k_{sk,1}^2} |p=2, \frac{k_{d,1}^2/k_{sk,1}^2 |p=2}{2 \sin^2 2\pi/Q_r} \\ \frac{k_{d,1}^2}{k_{sk,1}^2} |p=3, \frac{k_{d,1}^2/k_{sk,1}^2 |p=3}{2 \sin^2 3\pi/Q_r} \\ \frac{k_{d,1}^2}{k_{sk,1}^2} |p=6, \frac{k_{d,1}^2/k_{sk,1}^2 |p=6}{2 \sin^2 6\pi/Q_r} \end{bmatrix}}_{A_r} \underbrace{\begin{bmatrix} R_b \\ R_{er} \end{bmatrix}}_{\mathbf{x}_r}. \quad (13)$$

The closed-form solution to the WLS problem  $\min_{\mathbf{x}_r} \|W_1^{0.5} (A_r \mathbf{x}_r - \mathbf{b}_r)\|_2^2$  for (13) is provided in (14), where a diagonal weight matrix,  $W_1$ , is introduced. This ansatz is motivated in Section III-E, where the selection of the matrix is also formalized.  $W_1^{0.5}$  is interpreted as the element-wise square-root of  $W_1$ .

$$\hat{\mathbf{x}}_r = (A_r^T W_1 A_r)^{-1} A_r^T W_1 \mathbf{b}_r \quad (14)$$

Next,  $L_b$ ,  $L_{er}$ ,  $\Lambda_\sigma$  and  $L_{m,h}^{HPD}$  can be jointly estimated from (4), (6) and (13). The number of unknowns for the studied VPPM, whose  $n_{mw} = Q_s$ , is  $3 + \lceil n_{mw}/2 \rceil = 21$ . However, if only the fundamental time-harmonic is considered and tests are conducted for all viable three-phase configurations, the data vector contains  $n_{eq} = 3n_{PPC} = 12$  data points. Here,  $n_{eq}$  is the number of equations and  $n_{PPC}$  the number of PPCs for

which standard tests have been performed. These data points correspond to the VSD stator, magnetizing, and rotor-leakage inductances for the  $n_{PPC} = 4$  PPCs achievable with a three-phase connection of the studied VPPM. Hence, concatenating (4), (6) and (13) results in an underdetermined LES. Generally, the LES is underdetermined when  $n_{eq} < n_{PPC} + \lceil n_{mw}/2 \rceil / 3$ .

To make the problem well-posed, it can be formulated as a Tichonov regularization problem [23][p.101], where the pole-dependency of the magnetizing inductances, (5), is accounted for by a kernel relation through the matrix  $\Gamma$ . It incorporates the prior belief that  $L_{m,h}^{HPD}$  decreases as  $h^{-2}$ . By (6) and (11),  $L_{ss,p}^{VSD}$  can be related to  $\hat{L}_m^{HPD}$  and  $\Lambda_\sigma$  through matrices  $\mathbf{B}_{(1)}$  and  $\mathbf{B}_{(2)}$ . (15) defines the  $ij^{\text{th}}$  entries of  $\Gamma$  and  $\mathbf{B}_{(\cdot)}$ .

$$\Gamma_{k,k} = 1, \quad \Gamma_{k,k+1} = -(k+1/k)^2 \quad (15a)$$

$$\mathbf{B}_{(1) i,j} = k_{d,j}^2, \quad \text{if } j \in h_{1,p(i)} \quad (15b)$$

$$\mathbf{B}_{(2) i,j} = k_{d,j}^2, \quad \text{if } j = p(i) \quad (15c)$$

$k$  runs from 1 to  $Q_s/2 - 1$ , and  $i$  from 1 to  $n_{PPC}$ . All other entries in the matrices are set to zero. Finally, the LES is

$$\underbrace{\begin{bmatrix} L_{ss}^{VSD} \\ L_{rr}^{VSD} \\ L_m^{VSD} \\ \mathbf{0}_{Q_s/2-1} \end{bmatrix}}_{\mathbf{b}_s} = \underbrace{\frac{Q_s}{m_s} \begin{bmatrix} \mathbf{B}_{(1)} & z_Q^2 \mathbf{1}_{n_{PPC}} & \mathbf{0}_{n_{PPC}} \\ \mathbf{B}_{(1)} & \mathbf{0}_{n_{PPC}} & m/Q_s \mathbf{A}_r \\ \mathbf{B}_{(2)} & \mathbf{0}_{n_{PPC}} & \mathbf{0}_{n_{PPC}} \\ \Gamma & \mathbf{0}_{Q_s/2-1} & \mathbf{0}_{Q_s/2-1} \end{bmatrix}}_{A_s} \underbrace{\begin{bmatrix} \hat{L}_m^{HPD} \\ \Lambda_\sigma \\ L_b \\ L_{er} \end{bmatrix}}_{\mathbf{x}_s}. \quad (16)$$

This overdetermined LES of  $n_{eq} + Q_s/2 - 1$  equations may be interpreted as a Tichonov-regularized LSQ problem of (4) and (6). To see this, (16) is expressed in block-matrix form in (17).

$$\left[ \mathbf{b}_{(1)}^T \ ; \ \mathbf{0}_{Q_s/2-1}^T \right]^T = \left[ \mathbf{B}^{*T} \ ; \ \Gamma^{*T} \right]^T \mathbf{x}_s \quad (17)$$

The problem

$$\min_{\mathbf{x}_s} \|W_1^{0.5} (\mathbf{B}^* \mathbf{x}_s - \mathbf{b}_{(1)})\|_2^2 + \|W_2^{0.5} (\Gamma^* \mathbf{L}_m^{HPD})\|_2^2 \quad (18)$$

, where  $W_1^*$  is  $W_1$  repeated three times along the diagonal and  $W_2 = \rho I_{Q_s/2-1}$  imposes a scalar penalty on the regularization term, has the general solution

$$\hat{\mathbf{x}}_s = m_s / Q_s (\mathbf{B}^{*T} W_1^* \mathbf{B}^* + \Gamma^{*T} W_2 \Gamma^*)^{-1} \mathbf{B}^{*T} W_1^* \mathbf{b}_{(1)}.$$

It can be verified that the regularization matrix,  $\Gamma$ , makes the problem non-singular. It is also clear from (18) that the last term favors solutions that follow the presumed pattern, as any deviation from a  $h^{-2}$ -decay imposes a quadratic penalty.

Finally, (18) is an unconstrained optimization problem. However,  $\hat{L}_{rr}^{HPD}$  and  $\hat{L}_{ss}^{HPD}$  pose requirements on the values of  $\hat{L}_m^{HPD}$ . To obtain physically reasonable solutions, we should therefore enforce the following linear constraints  $\forall h$ :

$$[\hat{L}_{m,h}^{HPD} - \hat{L}_{m,h+1}^{HPD}, \hat{L}_{\sigma(\cdot),h}^{HPD}, \hat{L}_{m,h}^{HPD}]^T \geq 0 \quad (19)$$

### E. Selection of Weighting Matrix

In Section III-D, we proposed to solve a WLS problem to estimate T-equivalent parameters.  $W_1$  was introduced to weigh the importance of the measurements of different PPCs. It is known from ID theory that the optimal matrix (under certain assumptions) contains the inverse of the measurement variances along the diagonal [23][p. 165].

To decide the variances, consider  $L_{ss,p}^{VSD}$ , which is calculated from the one-phase reactive power,  $Q$ , and  $I_s$  as  $L_{ss,p}^{VSD} = Q/(\omega_s |I_s|^2)$ . The WT500 power analyzer used in Section IV computes  $Q$  as  $Q = U_s I_s \sin(\varphi)$  [24], where  $\varphi$  is the power-factor angle. A first-order MacLaurin approximation then yields the error propagation formulae, (20) and (21), for  $L_{ss}^{VSD}$  and  $Q$ . Here,  $\psi_s$  is the stator flux linkage.

$$\begin{aligned} \Delta L_{ss}^{VSD} &\approx \omega_s^{-1} (|\partial L_{ss}^{VSD}/\partial Q| \Delta Q + |\partial L_{ss}^{VSD}/\partial I_s| \Delta I_s) \\ &= |1/(\omega_s I_s^2)| \Delta Q - |2\psi_s| \Delta I_s \end{aligned} \quad (20)$$

$$\begin{aligned} \Delta Q &= |I_s \sin(\varphi)| \Delta U_s + |U_s \sin(\varphi)| \Delta I_s + \\ &|U_s I_s \cos(\varphi)| \Delta \varphi \end{aligned} \quad (21)$$

In the linear operating range,

$$I_s \propto p/k_{d,p}, \quad \psi_s \propto k_{d,p}/p, \quad \psi_s \approx U_s/\omega_s. \quad (22)$$

Additionally,  $\Delta U_s$  and  $\Delta I_s$  are proportional to the absolute value of the reading [24]. We further assume  $\varphi$  to be approximately the same for all pole configurations during the NL tests and that the machine saturates at the same air-gap magnetic field density. Substituting (21) and (22) into (20) and taking the variance under the assumption of uncorrelated measurement errors then renders (23).

$$\begin{aligned} \sigma_{L_{ss}}^2 &= [c_1 (k_{d,p}/p)^6 + c_2 (k_{d,p}/p)^2] \sigma_i^2 + \\ &c_3 (k_{d,p}/\omega_s p)^2 \sigma_u^2 + c_4 (k_{d,p}/p)^2 \sigma_\varphi^2 \end{aligned} \quad (23)$$

Here  $\sigma_{(\cdot)}$  denotes the variance of a measured quantity, and  $c_{(\cdot)}$  are constants for a given air gap field density. From (23), we conclude that  $\sigma_{L_{ss}}^2(p) \propto (k_{d,p}/p)^2$ , provided the first term becomes insignificant as compared to the others when  $p$  increases. Consequently, a measurement  $k$  in a  $p$ -pole pair configuration attains the weight  $W_{1,(k,k)} = (p/k_{d,p})^2$ .

#### IV. EXPERIMENTAL VSD AND VPPM MODEL PARAMETER-IDENTIFICATION

The VSD T-model parameters constitute the input data to the parameter IDs in Section III-D. Hence, standard NL and LR tests need to be performed in multiple winding configurations. We elaborate on how the VPPM parameters were experimentally identified and report the results in Section IV-A. In Section IV-B, the HPD parameters are computed from those results and the optimization proposed in Section III with  $\rho = 10$ . Hereinafter,  $\hat{(\cdot)}$  denotes an estimated parameter.

##### A. VSD Parameter Identification

The terminals were connected in turns to form  $[m_s = 3, p = \{1, 2, 3, 6\}]$  Y-configurations, corresponding to all achievable PPCs of the studied VPPM when  $m_s = 3$ . This was accomplished by rearranging the connections of the terminal box before connecting the  $m_s$  inputs to the inverter. For comparison, the default configuration is shown in Fig. 2, which gives independent excitation of each stator toroid. The three-phase voltage source inverter was connected to a 300 V DC-bus and modulated with sinusoidal PWM to supply the machine. Measurements were collected with a Yokogawa WT500 power analyzer. Although the proposed regularization, (18), allows for as few as one NL curve and two LR measurements, more data points typically lead to better statistical properties

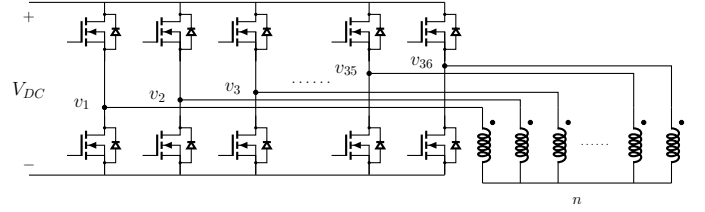


Fig. 2:  $Q_s = 36$ -leg inverter connected to the VPPM (default connection). Each coil is equipped with two terminals to allow for different winding configurations.

(e.g. variance) of the estimator, so we prefer to collect data for as many  $p$  as possible. Note, however, that we do not claim the suggested estimator to be efficient, nor consistent (see [25]).

First, the cold  $R_s^{VSD}$  was measured with an Ohm-meter connected across twelve series-connected coils.  $\hat{R}_s^{HPD} = 315 \text{ m}\Omega$  was computed as  $R_s^{VSD}/12$  to reduce variance. Due to the small  $R_s^{HPD}$ , contact and cabling resistance are potentially non-negligible once the machine is connected to the multiphase inverter after the parameter estimation. Therefore, a four-wire measurement was conducted between the inverter terminal and the terminal box to determine the average stray resistance between the machine toroids and the inverter outputs to 40 m $\Omega$ . This resistance should be added to the toroid resistance.

In practice, the voltage applied across the machine terminals differs from the reference voltage,  $u_{123}^{\text{ref}}$ , due to dead-time application, and the non-linear VI relationship of the inverter IGBTs. The combined effect of these voltage drops can be modeled as a current-dependent voltage source, (24) [26].

$$u_{123}(|i|) = u_{123}^{\text{ref}} - \text{sgn}(i) u_t(|i|) \quad (24)$$

To adjust for this voltage drop,  $u_{123}^{\text{ref}}$  from the current controller should be incremented by  $\text{sgn}(i) u_t(|i|)$  before the modulator to accomplish the desired voltage at the terminals. Experiments were conducted to determine  $u_t(|i|)$  for the inverter's Onsemi FNA23512a IGBT module and the result was stored in a lookup table. Accurate compensation is crucial when comparing experimental results to a simulated HPD model, particularly at low frequencies where  $u_{123}$  is small.

Next, conventional NL tests were performed in order to determine  $L_{\sigma s}^{VSD}$  and the unsaturated magnetizing inductance,  $L_{m0}^{VSD}$ , for each configuration using the so-called indirect method in [27]. It derives these parameters from the collected NL-curves with  $n_{exp}$  data points by minimizing the cost function in (25a). Due to the limited voltage supply, the frequency was decreased once the modulation index reached unity to saturate the machine. (25b) states the estimation of the magnetizing flux linkage, and (25c) the candidate model of  $L_m$ . The hyper-parameters  $\hat{\alpha}$  and  $\hat{a}$  relate to the flux-linkage saturation break-point and the steepness of the slope of  $\hat{L}_m(\hat{\psi}_m)$ . Because (25) is applicable for the estimation of both VSD and HPD parameters by means of NL tests, we have disposed of the superscripts.

$$J(\hat{L}_{m0}, \hat{\alpha}, \hat{a}, \hat{L}_{\sigma s}) = \sum_{k=1}^{n_{exp}} \left( \hat{L}_{m,k} - \hat{\psi}_{m,k}/i_{s,k} \right)^2 \quad (25a)$$

$$\hat{\psi}_m = \sqrt{u_s^2 - (R_s i_s)^2} / \omega_s - \hat{L}_{\sigma s} i_s \quad (25b)$$

$$\hat{L}_m(\hat{\psi}_m) = \hat{L}_{m0} / (1 + \hat{\alpha} \hat{\psi}_m^{\hat{a}}) \quad (25c)$$

TABLE I: VSD-parameters of the studied VPPM.

$p$	$\hat{L}_m^{VSD}$ [mH]	$\hat{L}_{\sigma r}^{VSD}$ [mH]	$\hat{L}_{\sigma s}^{VSD}$ [mH]	$\hat{R}_s^{VSD}$ [ $\Omega$ ]	$\hat{R}_r^{VSD}$ [ $\Omega$ ]
1	1733	51	50	3.80	2.37
2	441	21	49	3.80	1.57
3	208	30	33	3.80	1.45
6	61	31	17	3.80	1.49

TABLE II: Rotor parameters of the studied VPPM.

$\hat{R}_b$ [ $\mu\Omega$ ]	$\hat{R}_{er}$ [ $\mu\Omega$ ]	$\hat{L}_b$ [nH]	$\hat{L}_{er}$ [nH]
52.46	1.39	1091	22

The LR tests were conducted with a variable transformer at  $\omega_s = 100\pi \text{ rad}\cdot\text{s}^{-1}$  and the voltage was gradually raised until rated current was reached. Provided the results from the NL tests,  $R_r^{VSD}$  and saturated  $L_{r\sigma}^{VSD}$  can be calculated by solving the non-linear equation system in (26).

$$\text{Re}\{\underline{Z}_{in}\} = R_s^{VSD} + \alpha \quad (26a)$$

$$\text{Im}\{\underline{Z}_{in}\} = X_{\sigma s}^{VSD} + \beta \quad (26b)$$

$$\alpha = (ac+bd)/(a^2+b^2), \quad \beta = (ad-bc)/(a^2+b^2)$$

$$a = F_{sk,R}(\omega_s)R_r^{VSD}/s, \quad b = X_m^{VSD} + X_{\sigma r}^{VSD}F_{sk,L}(\omega_s)$$

$$c = -X_m^{VSD}X_{\sigma r}^{VSD}F_{sk,L}(\omega_s), \quad d = F_{sk,R}(\omega_s)X_m^{VSD}R_r^{VSD}/s$$

Above,  $X(\cdot) = \omega_s L(\cdot)$  denotes a reactance. The results of the parameter IDs are summarized in Table I.

### B. HPD Parameter Identification

Figs. 3 to 5 display the identified T-model parameters. The lower subplots show the HPD parameters as a function of  $h$ . In turn, the upper subplots compare the parameters obtained through the standard tests (transparent) with the equivalent VSD parameters obtained from (6), (7) and (11) using the identified parameters,  $\hat{\theta}$  (opaque). The numerical values above the bars refer to the equivalent parameters calculated from  $\hat{\theta}$ . The differences relative to the values in Table I are shown within parentheses. The rotor parameters from which Fig. 4 is generated through (8) are also listed in Table II. Notably,  $\hat{R}_{r,h}$  and  $\hat{L}'_{\sigma r,h}$  increase for higher number of  $h$ , due to the decreasing  $k_{sk,h}^{\text{HPD}}$  in (8). It is also discerned for  $R_r^{VSD}$  and  $L_{\sigma r}^{VSD}$  in Table I, which increase slightly for  $p = 6$  as compared to  $p = 3$ . The stator leakage inductance is computed from  $L_{\sigma s,6}^{VSD} = 26 \text{ mH}$ , Fig. 5, and the relations (4c) and (9):

$$\hat{L}_{\sigma s}^{\text{HPD}} = 2.2 \text{ mH}.$$

In Fig. 3, the experimentally identified  $L_{m,p}^{VSD}$  largely follow a  $1/p^2$ -trend but the rate of change decreases for lower  $p$ . For instance, if  $\hat{L}_{m,6}^{VSD}$  was extrapolated to find  $\hat{L}_{m,1}^{VSD}$  using (5), the result would be  $\hat{L}_{m,1}^{VSD} \approx 1.95 \text{ H}$ . This observation indicates that it is important to characterize a VPPM in all pole configurations and derive parameters for a suitable model taking both measurements and theory into account.

## V. EXPERIMENTAL MODEL VALIDATION

In this section, the HPD model using the inferred parameters is assessed relative to experimental results. First, the identified  $L_m^{\text{HPD}}$  and  $L_{\sigma s}^{\text{HPD}}$  are juxtaposed with the corresponding parameters derived from conventional NL-curves obtained by exciting the corresponding harmonic plane with a multiphase

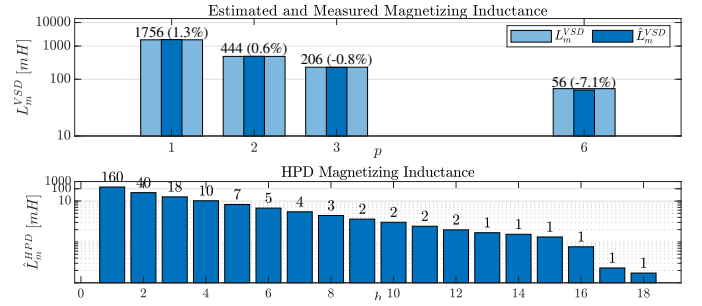


Fig. 3: Identified magnetizing inductances.

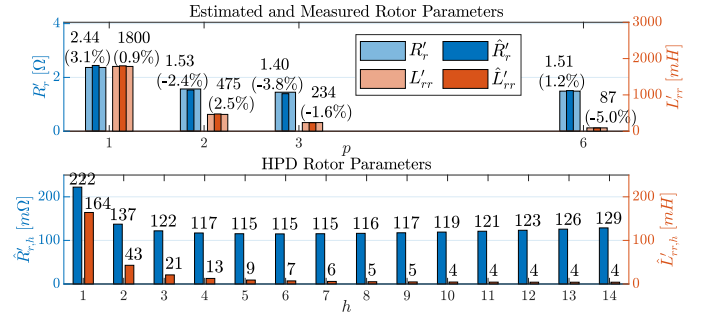


Fig. 4: Identified rotor inductances and resistances.

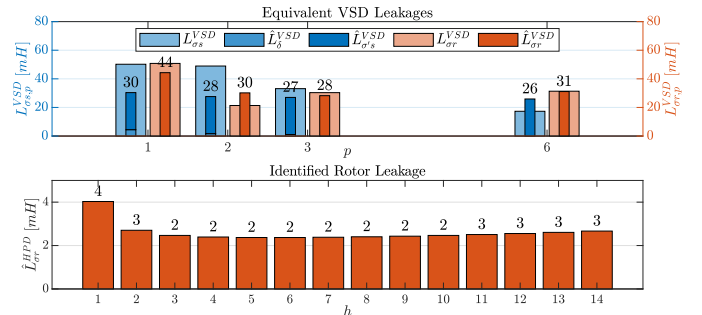


Fig. 5: Identified leakage inductances.

inverter, as proposed in [16]. Next, s.s behavior and pole-changing transients are assessed when applying  $\tau_L = 5 \text{ N}\cdot\text{m}$  of load torque. Finally, the correspondence between the torque reference issued by the VPPM speed controller,  $\tau_h^{\text{ref}}$ , and the measured shaft torque,  $\tilde{\tau}$ , is reported.

The terminal box was connected to independently excite the stator toroids, as shown in Fig. 2. The shaft of the VPPM was connected to a standard three-phase IM as depicted in Fig. 6. It was operated in torque-control mode with a commercial inverter. To measure the shaft torque, a Magtrol TM312 torque transducer was mounted between two shaft couplings and connected to a Magtrol 3411 torque display, as shown in Fig. 6. The VPPM was operated in PPCs with  $q_s = 1$  for  $h = 1, 2, \dots, 6$  and the resulting currents in the corresponding harmonic planes were recorded together with the speed.  $\mathbf{u}_{\alpha\beta,h}^{\text{ref}}$  and  $\omega_m$  were saved and used to excite an analytical model of the VPPM in MATLAB®/Simulink® with the identified parameters and implementing (2), as illustrated in Fig. 7. During the dynamic and loaded s.s experiments, the VPPM was operated in speed-control mode at 1001 rpm while magnetized with  $i_{sd,h}$  in the linear range.

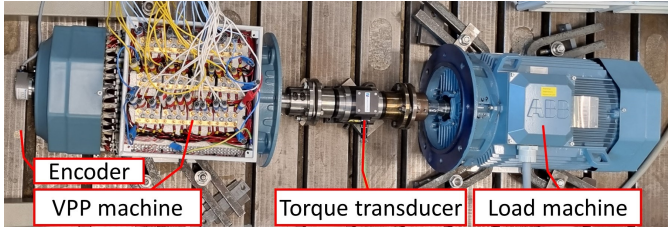


Fig. 6: VPPM test bench.

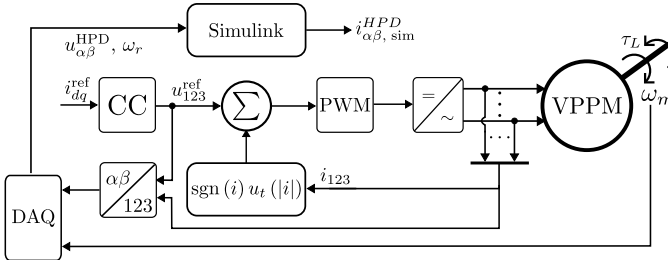


Fig. 7: Block diagram of the experimental setup. Details of the control are given in [2].

### A. Validation Using NL Curves

Conventional NL-curves were captured by exciting  $h \in \{1, 2, 3, 4\}$ , one at a time, using a multiphase inverter. The machine was operated in speed-control mode at 1001 rpm using controllers tuned with the parameters declared in Section IV-B [2]. Different references for  $i_{sd,h}$  were commanded to change the magnetization.

The indirect method proposed in [27] and described by (25) is employed again for each harmonic plane to identify  $\hat{L}_{m,h}^{\text{HPD}}$  and  $\hat{L}_{\sigma s,h}^{\text{HPD}}$ . The estimated HPD parameters are to be compared to the values obtained from the WLS estimation in Section IV-B. It is noted that  $i_s \approx i_m$  at NL, provided low slips. Consequently,  $\hat{L}_m \approx \psi_m/i_s$ . The slip was measured to 1.0, 1.5, 1.9, and 2.2% for  $h = 1, 2, 3$ , and 4, respectively, at the lowest magnetization. Current transducers and a DAQ-system were used to measure  $\omega_s$  of  $i_{s,h}$  and a tachometer to measure  $\omega_m$ .

Fig. 8 plots  $\hat{L}_{m,h}(\hat{\psi}_{m,h})$  resulting from the optimizations.  $\psi_m$  has been normalized such that  $\hat{\psi}_m = 1$  pu when  $\hat{L}_m(\hat{\psi}_m) = 0.9\hat{L}_{m0}$ . Additionally, the parameters corresponding to each curve fit have been tabulated.

For  $\hat{\psi}_m \lesssim 0.5$  pu,  $\hat{L}_m$  appears to decrease. The explanation is two-fold. Firstly,  $i_{s,h} \approx i_{m,h}$  is a worse approximation when  $s_h$  increases. The impact is greater, the higher the pole number,

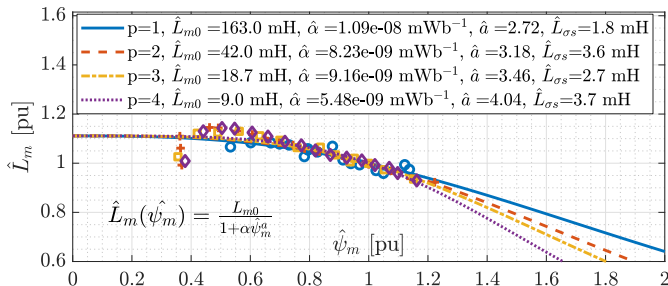

 Fig. 8: NL curves for  $h = 1, 2, 3, 4$ . Markers correspond to data points, whereas lines are the fitted saturation model (25c).

TABLE III: Errors in current amplitude and phase of the identified HPD model compared to experimental data at 4.9 N·m loaded s.s.

h	1	2	3	4	5	6
$( \hat{i}_{s\alpha\beta,h}  -  i_{s\alpha\beta,h} ) /  i_{s\alpha\beta,h} $ [%]	-10.7	2.8	3.6	0.9	-8.0	-9.8
$\hat{\varphi}_h - \varphi_h$ [°]	-8.0	-4.3	-2.0	-1.0	-2.0	-0.2

due to (5). This affects the estimation (25b), which is no longer a real number. Consequently,  $\hat{L}_m$  is underestimated. Secondly, the M250-35A steel of the machine exhibits a decreasing relative permeability at flux densities below 0.3 T [28].

Comparing  $\hat{L}_{m0,h}$  and  $\hat{L}_{\sigma s,h}$  in Fig. 8 to the values of  $\hat{L}_{m,h}^{\text{HPD}}$  and  $\hat{L}_{\sigma s,h}^{\text{HPD}} = 2.2$  mH obtained in Section IV suggests that the WLS-method renders estimations of the stator inductance parameters that are very similar to the parameters obtained through the standard NL tests performed for each harmonic plane individually. It is noted that it becomes prohibitive to run the NL tests as  $h$  increases, due to the vanishing  $L_{m,h}$ . Likewise, LR tests are not viable.

### B. Validation at Loaded Steady-State and PPC Transition

Fig. 9 displays experimental s.s currents of the evaluated PPCs together with the simulated counterparts. Table III lists the errors of the simulated fundamental space-vector amplitude and phase, found from an FFT.

A phase-pole transition constitutes an electro-mechanical transient, which requires an accurate model. It is an important feature of a VPPM, as it allows to switch operating points, similar to a gearbox. Transitions are executed in three steps encompassing a demagnetization of the initial PPC,  $h^{(1)}$ , a premagnetization of the subsequent PPC,  $h^{(2)}$ , and a switch of  $i_{sq,h}^{\text{ref}}$  from  $h^{(1)}$  to  $h^{(2)}$ . More details are provided in [2].

During a transition, two phenomena that may affect the accuracy of the simulations should be considered. Firstly, magnetic cross-saturation may occur when superimposing two magnetic fields [29]. The implemented pole-changing strategy was elaborated to mitigate this effect [2], but it is difficult to model and may still inflict saturation in parts of the machine.

Secondly, the flux-transients compel the machine to operate at high slip during the transitions as a decrease in flux requires more q-current to retain the torque and vice versa. Hence, the skin effect becomes pronounced. A fair comparison to the experiments requires that the simulation model incorporates the skin effect. To that end,  $F_{sk,R}$  and  $F_{sk,L}$  are calculated at each time step of the simulation, which requires that  $\omega_{sl}$  is estimated. We choose to employ (27) as an estimator. The rationale for the expression is that  $\theta_e = \text{atan} \psi_{R\beta,h} / \psi_{R\alpha,h}$ , whose low-pass filtered derivative,  $\hat{\omega}_e$ , is the first term in (27).  $x_h$  and  $y_h$  are the simulated  $\psi_{R,h}^s$  passed through a low-pass filter with time constant  $\tau_f$  in Laplace domain.

$$\hat{\omega}_{sl} = \frac{(x_h \frac{d^2 y_h}{dt^2} - y_h \frac{d^2 x_h}{dt^2}) / (x_h^2 + y_h^2) - \dot{h} \omega_m}{x_h(s) = \psi_{R\alpha,h}(s) / (\tau_f s + 1), \quad y_h(s) = \psi_{R\beta,h}(s) / (\tau_f s + 1)} \quad (27)$$

Experimental results for a set of viable transitions are shown in Fig. 10 alongside the simulated currents for identical excitation.  $h^{(1)}$  and  $h^{(2)}$  are chosen to avoid radial bearing stress in the transitions, which arise if  $|h^{(1)} - h^{(2)}| = 1$  [3].

Fig. 10 indicates that the HPD model adopting the estimated

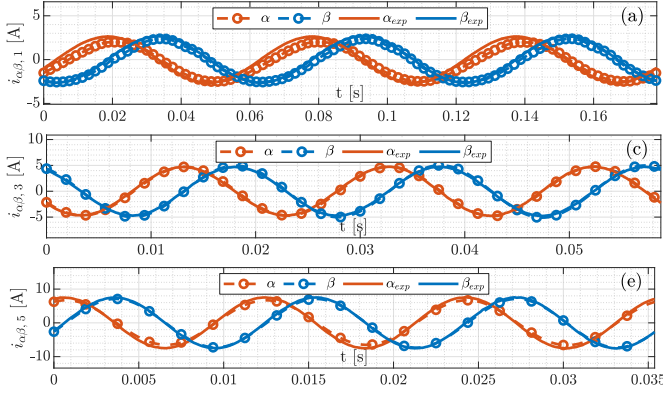


Fig. 9: Current waveforms at s.s. of the simulated HPD-model compared to experimental data of a 5 N·m loaded VPPM. (a)  $h = 1$ , (b)  $h = 2$ , (c)  $h = 3$ , (d)  $h = 4$ , (e)  $h = 5$ , (f)  $h = 6$ .

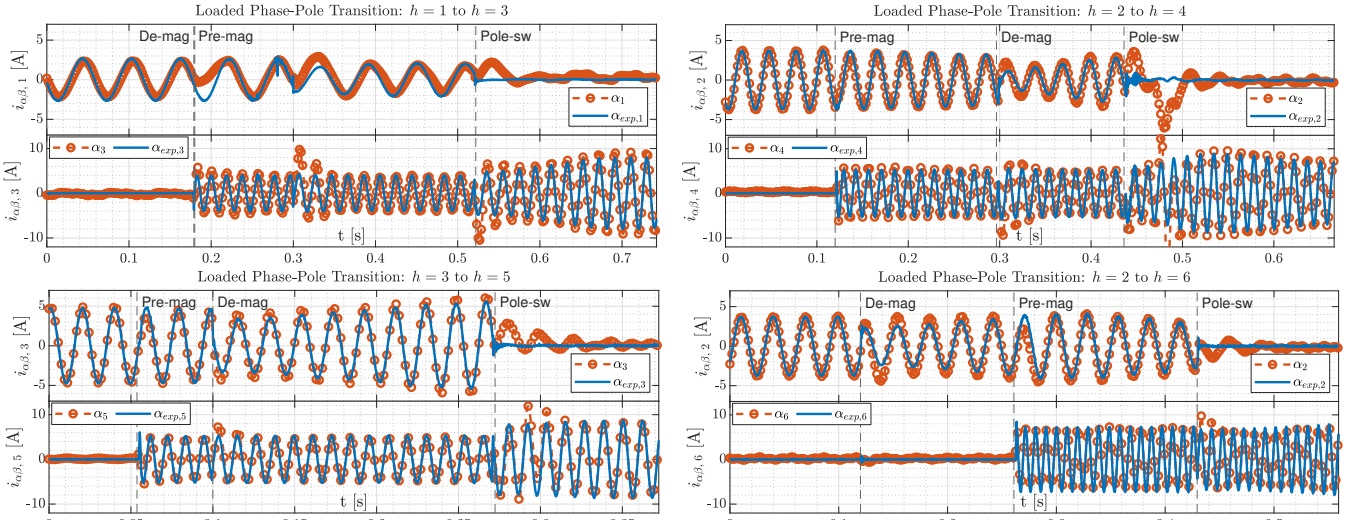


Fig. 10: Experimental currents for loaded phase-pole transitions (solid) compared to the simulated HPD model (markers).

parameters agrees well to the measured currents. We remark that the currents in the unexcited harmonic planes are regulated to zero, as per best practice in multiphase machines [13]. Consequently, non-zero voltage are impressed to compensate for imbalances and non-linearities in the drive that else would cause a current. The model does not include such imperfections, whereby a residual current results in the simulated (typically low-impedance) circuit, as visible in Fig. 10.

### C. Validation of Torque-Reference Linearity

Fig. 11 plots  $\tau_h^{\text{ref}}$  against  $\tilde{\tau}$  for  $h = 1, 2, 3, 4$ . The solid lines comprise LSQ fits of the measured data, indicated with markers. At s.s. and with perfect rotor field orientation, (28) relates  $\tau_h^{\text{ref}}$ , commanded by the speed controller, to  $i_{sq,h}^{\text{ref}}$  of the single torque-generating plane.

$$i_{sq,h}^{\text{ref}} = 4(L_{m,h} + L'_{\sigma r,h})\tau_h^{\text{ref}} / (Q_s h L_m^2 i_{sd}^{\text{ref}}) \quad (28)$$

Ideally,  $\tau_h^{\text{ref}} = \tilde{\tau}$  (accounting for frictional losses) but imperfections in the field orientation and in calculating the correct  $i_{sq,h}^{\text{ref}}$  due to parameter inaccuracies cause the lines to deviate. Therefore, the linearity of the curves and the correspondence to the ideal curve provide some suggestions as to how accurate the parameters are.  $i_{sq,h}^{\text{ref}} \propto \tau_h^{\text{ref}}$  holds as long as linear

magnetic conditions prevail. Otherwise,  $L_{m,h}$  changes with  $i_{sd,h}^{\text{ref}}$  and  $i_{sq,h}^{\text{ref}}$  needs to compensate for the saturation in rotor flux linkage to output the torque required to retain the desired speed. Therefore, the experiments were conducted with a fixed magnetization,  $i_{sd,h}^{\text{ref}}$ , below the saturation breakpoint as indicated in the figure caption.

The coefficients of determination,  $R^2$ -values, of the LSQ fits reported in Fig. 11 suggest a high degree of linearity in all four harmonic planes. It is seen that the slopes of the regression lines deviate from one, which implies some degree of parameter inaccuracy (and/or measurement errors). However, the discrepancies are considered acceptable.

## VI. CONCLUSION

An offline parameter identification method for variable phase-pole machines (VPPMs) adopting a harmonic plane decomposition (HPD) model was proposed. It formulates a constrained, regularized weighted least-squares problem provided data from standard tests. The tests are conducted with fundamental excitation and can be performed with a sinusoidal three-phase source. Parameters of a VPPM were experimentally identified. The inferred HPD model was simulated and

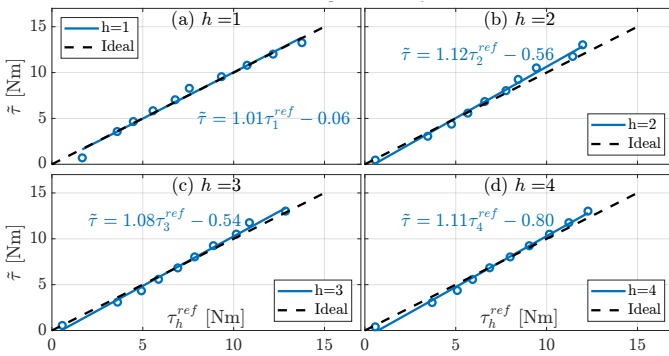


Fig. 11: Torque reference versus measured shaft torque. The  $R^2$ -values of the linear fits are (a) 0.9862, (b) 0.9925, (c) 0.9927, and (d) 0.9944. The  $i_{sd,h}^{ref}$  were (a) 1.5 A, (b) 2.6 A, (c) 3.9 A, and (d) 5.9 A.

compared to experiments for loaded steady-state and phase-pole transitions. No-load curves were elaborated for each harmonic plane and were compared to the parameters from the proposed method. The validations showed good agreement. The case study indicates that it is important to perform tests in multiple pole configurations and weigh these measurements appropriately to obtain accurate HPD parameters.

## REFERENCES

[1] Y. Zhao and T. A. Lipo, "Space vector PWM control of dual three-phase induction machine using vector space decomposition," *IEEE Transactions on Industry Applications*, vol. 31, no. 5, pp. 1100–1109, 1995.

[2] Y. Wu, G. Falk Olson, and L. Peretti, "Pole-transition control of variable phase-pole machines using harmonic-plane decomposition," *TIE Transactions on Industrial Electronics*, vol. Early Access, pp. 1–8, 2023, doi:10.1109/TIE.2022.3231328.

[3] M. Osama and T. A. Lipo, "Modeling and analysis of a wide-speed-range induction motor drive based on electronic pole changing," *IEEE Transactions on Industry Applications*, vol. 33, no. 5, pp. 1177–1184, 1997.

[4] K. Bitsi, O. Wallmark, and S. Bosga, "An induction machine with wound independently-controlled stator coils," in *2019 22nd International Conference on Electrical Machines and Systems (ICEMS)*, Conference Proceedings, pp. 1–5.

[5] G. Dajaku and D. Gerling, "Low costs and high efficiency asynchronous machine with stator cage winding," in *2014 IEEE International Electric Vehicle Conference (IEVC)*, Conference Proceedings, pp. 1–6.

[6] E. Libbos, B. Ku, S. Agrawal, S. Tungare, A. Banerjee, and P. T. Krein, "Loss minimization and maximum torque per ampere operation for variable-pole induction machines," *IEEE Transactions on Transportation Electrification*, pp. 1–1, 2020.

[7] E. Libbos, E. Krause, A. Banerjee, and P. T. Krein, "Inverter design considerations for variable-pole induction machines in electric vehicles," *IEEE Transactions on Power Electronics*, vol. 37, no. 11, pp. 13554–13565, 2022.

[8] Y. Matsuyama, K. Ishizuka, T. Kosaka, H. Matsumori, and N. Matsui, "Design study on high torque density multiphase pole-change induction motor for vehicle propulsion drive," in *2021 24th International Conference on Electrical Machines and Systems (ICEMS)*, 2021, pp. 426–431.

[9] B. P. Reddy, A. Iqbal, S. Rehman, M. Meraj, and S. Keerthipati, "Dynamic modelling and control of pole-phase modulation based multiphase induction motor drives," *IEEE Journal of Emerging and Selected Topics in Power Electronics*, pp. 1–1, 2021.

[10] M. P. Magill, P. T. Krein, and K. S. Haran, "Equivalent circuit model for pole-phase modulation induction machines," in *2015 IEEE International Electric Machines Drives Conference (IEMDC)*, 2015, pp. 293–299.

[11] Y. Wang, J. Yang, R. Deng, and G. Yang, "Parameters estimation for multiphase induction machine with concentrated windings through finite element method," *IET Electric Power Applications*, vol. 14, no. 10, pp. 1807–1817, 2020.

[12] J. A. Riveros, A. G. Yepes, F. Barrero, J. Doval-Gandoy, B. Bogado, O. Lopez, M. Jones, and E. Levi, "Parameter identification of multiphase induction machines with distributed windings - part 2: Time-domain techniques," *IEEE Transactions on Energy Conversion*, vol. 27, no. 4, pp. 1067–1077, 2012.

[13] A. G. Yepes, J. A. Riveros, J. Doval-Gandoy, F. Barrero, Ó. Lopez, B. Bogado, M. Jones, and E. Levi, "Parameter identification of multiphase induction machines with distributed windings - part 1: Sinusoidal excitation methods," *IEEE Transactions on Energy Conversion*, vol. 27, no. 4, pp. 1056–1066, 2012.

[14] W. Kong, J. Huang, R. Qu, M. Kang, and J. Yang, "Nonsinusoidal power supply analysis for concentrated-full-pitch-winding multiphase induction motor," *IEEE Transactions on Industrial Electronics*, vol. 63, no. 1, pp. 574–582, 2016.

[15] A. S. Abdel-Khalik, R. A. Hamdy, A. M. Massoud, and S. Ahmed, "Low-order space harmonic modeling of asymmetrical six-phase induction machines," *IEEE Access*, vol. 7, pp. 6866–6876, 2019.

[16] A. Abdelkhalik, M. Masoud, and W. Barry, "Eleven-phase induction machine: steady-state analysis and performance evaluation with harmonic injection," *IET Electric Power Applications*, vol. 4, no. 8, pp. 670–685, 2010.

[17] Y. Wu, A. Pisani, G. Falk Olson, K. Bitsi, O. Wallmark, and L. Peretti, "FEM-based parameter estimation for a variable phase-pole induction machine," in *2021 23rd European Conference on Power Electronics and Applications (EPE'21 ECCE Europe)*, 2021, pp. P.1–P.10.

[18] G. Falk Olson and L. Peretti, "Parameter estimation of multiphase machines applicable to variable phase-pole machines," in *2022 International Conference on Electrical Machines (ICEM)*, 2022, pp. 949–955.

[19] M. P. Magill and P. T. Krein, "A dynamic pole-phase modulation induction machine model," in *2015 IEEE International Electric Machines & Drives Conference (IEMDC)*, Conference Proceedings, pp. 13–19.

[20] A. A. Rockhill and T. A. Lipo, "A generalized transformation methodology for polyphase electric machines and networks," in *2015 IEEE International Electric Machines & Drives Conference (IEMDC)*, Conference Proceedings, pp. 27–34.

[21] J. Pyrhonen, T. Jokinen, and V. Hrabovcov, *Design of Rotating Electrical Machines*. John Wiley & Sons, Ltd, 2013, ch. 7, pp. 331–494.

[22] D. G. Holmes and T. A. Lipo, *Pulse Width Modulation for Power Converters: Principles and Practice*, 2003, ch. 2, pp. 57–94.

[23] Å. Björck, *Numerical Methods for Least Squares Problems*. Society for Industrial and Applied Mathematics, 1996. [Online]. Available: <https://epubs.siam.org/doi/abs/10.1137/1.9781611971484>

[24] Yokogawa Test and Measurement Corporation, "WT500 power analyzer user's manual," 2019. [Online]. Available: <https://cdn.tmi.yokogawa.com/1/5959/files/IM760201-01E.pdf>

[25] L. Ljung, *System Identification Theory for the User*. Upper Saddle River, NJ, USA: Prentice Hall PTR, 1999.

[26] L. Peretti and M. Zigliotto, "Automatic procedure for induction motor parameter estimation at standstill," *IET Electric Power Applications*, vol. 6, no. 4, pp. 214–224, 2012.

[27] T. Tuovinen, M. Hinkkanen, and J. Luomi, "Modeling of mutual saturation in induction machines," in *2008 IEEE Industry Applications Society Annual Meeting*, 2008, pp. 1–8.

[28] Tata Steel Europe, "Typical data for sura m250-35a," 2008. [Online]. Available: <https://www.tatasteeleurope.com/sites/default/files/m250-35a.pdf>

[29] J. Milos, B. Brkovic, E. Levi, and Z. Lazarevic, "Interplane cross-saturation in multiphase machines," *IET Electric Power Applications*, vol. 13, no. 11, p. 1812–1822, 2019.

## VII. BIOGRAPHIES



**Gustaf Falk Olson** was born in Kristinehamn, Sweden. He received his M.Sc. in electrical power engineering from the Royal Institute of Technology KTH, Stockholm, Sweden in 2016. After graduation, he worked as a Field Application Engineer for Texas Instruments. Since 2019, he is working towards a Ph.D. in parameter estimation of multiphase electrical machines at the Division for Electrical Power and Energy Systems (EPE) at KTH Royal Institute of Technology, Stockholm, Sweden. His research encompasses modeling, control, and parameter estimation of multiphase machines.



**Yixuan Wu** received his M.Sc. in electrical engineering from the RWTH Aachen University, Aachen, Germany and KTH Royal Institute of Technology, Stockholm, Sweden in 2019. Since 2019, he is working towards a Ph.D. in fault tolerance of multiphase electrical machines at the Division for Electrical Power and Energy Systems (EPE) at KTH Royal Institute of Technology, Stockholm, Sweden. His research encompasses modeling and control of variable phase-pole drives, power electronics, fault-tolerance and electromobility.



**Luca Peretti** received the M.Sc. degree in Electronic Engineering in 2005 from the University of Udine, Italy, and the Ph.D. degree from the University of Padova, Italy, in 2009. Between November 2007 and March 2008, he was a visiting Ph.D. student at ABB Corporate Research, Västerås, Sweden. From August 2010 to August 2018, he was with ABB Corporate Research, Västerås, Sweden in different roles as principal scientist, project leader and strategy coordinator. He has also been an Affiliated Faculty member at KTH, division of Electric Power and Energy Systems, since July 1, 2016. From September 2018 Luca is an Associate Professor at KTH, division of Electric Power and Energy Systems, in the field of Electric Machines and Drives. His main scientific interests relate to the automatic parameter estimation in electric machines, sensorless control, loss segregation in drive systems, multiphase drives, condition monitoring of machines and drives, in the context of industrial, wind energy, and traction applications.